

# Nonlinear reconnecting edge localized modes in current-carrying plasmas

F. Ebrahimi

Citation: *Physics of Plasmas* **24**, 056119 (2017); doi: 10.1063/1.4983631

View online: <http://dx.doi.org/10.1063/1.4983631>

View Table of Contents: <http://aip.scitation.org/toc/php/24/5>

Published by the [American Institute of Physics](#)

---

## Articles you may be interested in

[Extended MHD modeling of tearing-driven magnetic relaxation](#)

*Physics of Plasmas* **24**, 056107 (2017); 10.1063/1.4977540

[Structure and structure-preserving algorithms for plasma physics](#)

*Physics of Plasmas* **24**, 055502 (2017); 10.1063/1.4982054

[Key results from the first plasma operation phase and outlook for future performance in Wendelstein 7-X](#)

*Physics of Plasmas* **24**, 055503 (2017); 10.1063/1.4983629

[Impact of toroidal and poloidal mode spectra on the control of non-axisymmetric fields in tokamaks](#)

*Physics of Plasmas* **24**, 056117 (2017); 10.1063/1.4982688

[Impact of  \$E \times B\$  shear flow on low-n MHD instabilities](#)

*Physics of Plasmas* **24**, 050704 (2017); 10.1063/1.4984257

[Recent progress of magnetic reconnection research in the MAST spherical tokamak](#)

*Physics of Plasmas* **24**, 056108 (2017); 10.1063/1.4977922

---



## VACUUM SOLUTIONS FROM A SINGLE SOURCE

Pfeiffer Vacuum stands for innovative and custom vacuum solutions worldwide, technological perfection, competent advice and reliable service.

# Nonlinear reconnecting edge localized modes in current-carrying plasmas

F. Ebrahimi<sup>a),b)</sup>

Princeton Plasma Physics Laboratory and Department of Astrophysical Sciences, Princeton University, Princeton, New Jersey 08544, USA

(Received 27 March 2017; accepted 3 May 2017; published online 22 May 2017)

Nonlinear edge localized modes in a tokamak are examined using global three-dimensional resistive magnetohydrodynamics simulations. Coherent current-carrying filament (ribbon-like) structures wrapped around the torus are nonlinearly formed due to nonaxisymmetric reconnecting current sheet instabilities, the so-called peeling-like edge localized modes. These fast growing modes saturate by breaking axisymmetric current layers isolated near the plasma edge and go through repetitive relaxation cycles by expelling current radially outward and relaxing it back. The local bi-directional fluctuation-induced electromotive force (emf) from the edge localized modes, the dynamo action, relaxes the axisymmetric current density and forms current holes near the edge. The three-dimensional coherent current-carrying filament structures (sometimes referred to as 3-D plas-moids) observed here should also have strong implications for solar and astrophysical reconnection.

Published by AIP Publishing. [<http://dx.doi.org/10.1063/1.4983631>]

## I. INTRODUCTION

The magnetohydrodynamic (MHD) stability of the plasma boundary is critical for the successful performance of future magnetic fusion devices, such as ITER.<sup>1</sup> Quasiperiodic burst-like edge MHD instabilities observed routinely in the high performance operation regime of tokamaks, the H-mode,<sup>2</sup> have been shown to degrade the global confinement. Due to the formation of a transport barrier during H-mode operation, steep pressure gradients and large currents exist at the plasma edge, which could provide free energy for the so-called Edge Localized Modes (ELMs).<sup>3</sup> The quasiperiodic bursts of ELMs lead to the loss of energy and particles on short time scales of 0.1–1 ms and could potentially damage vessel components due to high local heat fluxes. ELMs are known to be ideal-like MHD modes of coupled peeling (current-driven) and ballooning (pressure-driven) instabilities.<sup>4,5</sup> Ideal (i.e., non-resistive) MHD codes, as well as extended MHD codes,<sup>6,7</sup> have been extensively used for linear studies of these modes. However, the effect of collisions as well as *full* nonlinear 3-D MHD dynamics of these modes has not yet been explored. In particular, the physics of their repetitive cycles has not been understood until now.

In this paper, we explore the nonlinear dynamics of current-driven ELMs using extended MHD simulations in a toroidal tokamak configuration. Understanding the physical dynamics, as well as poloidal/toroidal localization and the radial extent of these structures, is crucial for mitigating their impact. To shed light on the role of reconnection in ELM nonlinear dynamics, we here focus on the effect of finite edge current density. In the presence of resistivity, physical current layers developing near the plasma edge can be unstable to 3-D current-sheet instability.<sup>12</sup> Here, for the first time, coherent current carrying filament edge localized structures

with repetitive nonlinear dynamics are demonstrated during nonlinear MHD resistive simulations in a spherical tokamak. First, we perform simulations with varying toroidal magnetic fields ( $B_\phi$ ), but keeping the current-density profile fixed, and find that the growth of current-driven reconnecting edge localized modes (with tearing parity) scales with  $J_\parallel/B$  and stabilization occurs at high  $B_\phi$ . Second, we then show that these reconnecting edge modes with low toroidal mode numbers ( $n = 1 - 5$ ) saturate and form nonaxisymmetric filament current-carrying structures during the nonlinear stage. These nonlinear structures go through quasiperiodic oscillations. Third, we explain the physics of the nonlinear dynamics of the field-aligned filaments via direct calculations of the fluctuation induced emf term, the vector product of flow, and magnetic field fluctuations. The emf terms are localized around the edge current layers, where the reconnecting edge modes are triggered. It is also found that the current-driven edge modes alone (an important component of ELMs), without the pressure-driven component, are sufficient to explain the quasiperiodic cycles along with the rapid relaxation of edge current with a time scale of the order of 0.1 ms. The coherent filament structures found here are in particular very similar to the experimentally observed current-carrying filaments from peeling modes in Pegasus spherical tokamaks.<sup>8</sup> Filament structures in ELMs have been experimentally observed in other low-aspect ratio spherical tokamaks, MAST,<sup>9</sup> and NSTX.<sup>10</sup>

Edge localized peeling modes are triggered due to strong edge currents. In tokamaks, finite edge current density typically exists either due to the finite edge temperature (allowing Ohmic current flows) or finite edge pressure gradient (allowing bootstrap currents).<sup>3</sup> In this study, the edge currents are formed during the plasma startup current drive using the electrostatic helicity injection technique called Coaxial Helicity Injection (CHI), the primary candidate for non-inductive plasma current start-up in NSTX-U.<sup>11</sup> We show that the driven current structure at the edge of the injected flux could trigger current-driven edge localized modes.

Note: Paper D12 4, Bull. Am. Phys. Soc. 61, 116 (2016).

<sup>a)</sup>Invited speaker.

<sup>b)</sup>Electronic mail: ebrahimi@princeton.edu

Plasma generated during helicity injection current start up provides a unique platform to study the nonlinear evolution of edge localized current-driven instabilities in tokamaks in isolation, without the influence of other types of instabilities (pressure-driven ballooning). Although only the effect of finite edge current density is studied here using a CHI-like target, the parameter range studied covers conventional H-mode tokamak operation. Simulations have a local edge Lundquist number as high as  $5 \times 10^5$ , in the range of collisionalities of standard tokamak operation.

In addition to tokamaks, current-carrying intertwining flux-tubes emerging from the surface of the sun could also be similarly unstable to 3-D current-sheet instabilities.<sup>12</sup> In solar and astrophysical plasmas, magnetic reconnection could occur as a result of multiple current sheets.<sup>13</sup> These fast occurring reconnecting plasmas, such as solar flares on the surface of sun, are accompanied by magnetic helicity injection. Magnetic helicity, a measure of the knottedness and the twistedness of magnetic fields, could be injected through the twisting of magnetic field lines in the corona region via the relative shear motion of their foot points, with a helicity injection rate of  $\frac{\partial K}{\partial t} = -2 \int (\mathbf{A} \cdot \mathbf{V}) \mathbf{B} \cdot d\mathbf{s}$ <sup>14,15</sup> This field line twisting during helicity injection could bring the oppositely directed field lines together to form current sheets and eventually to cause reconnection. Similarly, in this study, current sheets are also formed during helicity injection. However, here, magnetic helicity is injected by applying current along the open field lines rather than through the relative shear motion of foot points of the open field lines. The helicity injection rate in this case is  $\frac{\partial K}{\partial t} = -2 \int \Phi \mathbf{B} \cdot d\mathbf{s}$ , which represents the intersection of a field line with a surface held at a constant electric potential. In both the cases, current sheets (or edge current layers) could be unstable to 3-D kink-like<sup>16</sup> or tearing-like current-sheet instabilities.<sup>12</sup> In the presence of resistivity, we show here that the current sheets can break to form coherent current-carrying filament structures (also sometimes known as 3-D plasmoids<sup>17</sup>).

This paper is organized as follows. The computational model is described in Sec. II. The simulation results in the growth phase of reconnecting edge localized modes are presented and discussed in Section III. The results of 3-D simulations during the nonlinear stage and the formation of 3-D coherent current structures are discussed in Section IV. The repetitive cycles are explained through edge current relaxation dynamics in Section V. We then summarize the main results in Sec. VI.

## II. THE MODEL

As described above, to study the effect of finite edge current density, we use a CHI-like target. We should note here that we do not intend to study the optimization of transient CHI for maximum flux closure, and we only use the target to form an initial plasma current non-inductively. The startup plasma current is formed by injecting biased poloidal flux, i.e., by driving current along the injected open field lines (the injector current) in the presence of an external toroidal field, shown in Fig. 1 (for details, also see Fig. 1 in Ref. 18). Helicity injection for current startup is initiated by

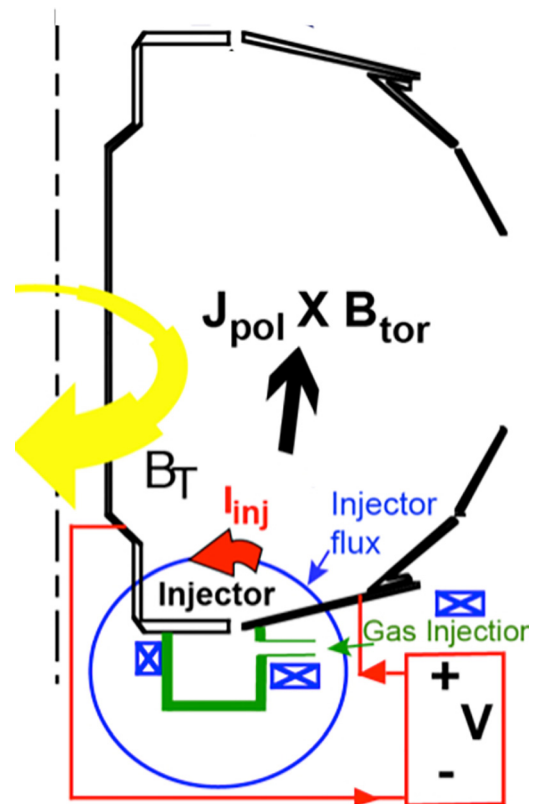


FIG. 1. Main components for non-inductive start-up current drive using helicity injection. In the presence of a toroidal field, current,  $I_{inj}$ , is driven along the open field lines (initial poloidal injector flux is shown in blue).

applying a voltage ( $V_{inj}$ ), or a constant electric field, to the divertor plates (the poloidal flux footprints). Helicity is injected through the linkage of resulting toroidal flux with the poloidal injector flux. Plasma and open field lines (the magnetic bubble) expand into the vessel if the injector current exceeds a threshold value. Figure 2(a) shows the typical expanded poloidal flux. As the poloidal flux is expanded in the volume, an edge current sheet at the edge of the injected flux is formed (Fig. 2). This edge current density layer is formed on both the high and low field sides of the tokamak as seen in Fig. 2(b). The current profile, although hollow in the core during the CHI, does have a peak near the edge, which could provide the free energy for nonaxisymmetric edge instabilities studied here. The current density spikes generated non-inductively here (Fig. 2(b)) are similar to the edge current spikes in ELMs in tokamaks.

To examine the nonlinear evolution of current-driven edge localized instabilities, we perform nonlinear MHD simulations using the NIMROD code.<sup>19</sup> We use a poloidal grid with  $45 \times 90$  fifth-order finite elements in a global  $(R, Z)$  geometry and toroidal Fourier mode numbers  $n \neq 0$  up to 43 in 3-D simulations. A uniform number density of  $4 \times 10^{18} \text{m}^{-3}$  for a deuterium plasma is used. The helicity injection model, boundary condition, and NSTX/NSTX-U geometries are the same as in previous papers.<sup>11,20,21</sup> Perfectly conducting boundary conditions with no-slip are used, except at the injector gap, which have a normal  $\mathbf{E} \times \mathbf{B}$  flow where a constant-in-time electric field is applied. To isolate the effect of current-driven

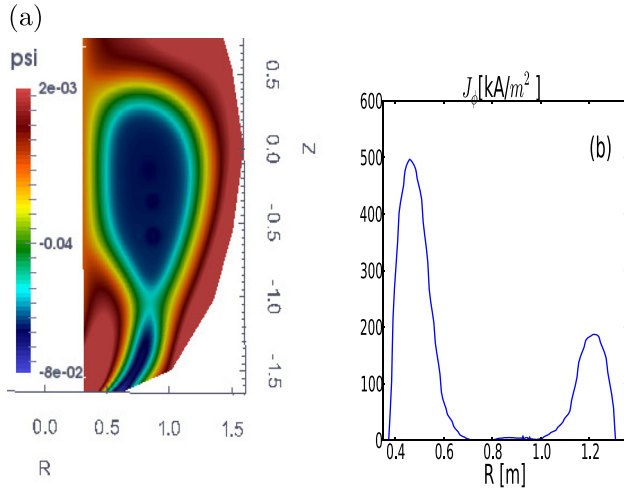


FIG. 2. Typical poloidal flux (Wb) and axisymmetric toroidal current density,  $J_\phi$  ( $\text{A/m}^2$ ), during nonlinear simulations.

instabilities localized near the edge, we perform resistive MHD simulations for the zero pressure model (pressure is not evolved in time). Any edge pressure-driven instabilities, including ballooning modes, are therefore eliminated here. We used magnetic diffusivities in the range of  $\eta = 2.5 - 12 \text{ m}^2/\text{s}$  to obtain the Lundquist number in the range of  $S = LV_A/\eta = 1 - 5 \times 10^5$ . Here, the Alfvén velocity  $V_A$  is based on the reconnecting magnetic field, and  $L$  is the current sheet length. The kinematic viscosities are chosen to give a  $\text{Pm} = 7.5$  (Prandtl number  $= \nu/\eta$ ).

We first perform three-dimensional simulations with the initial poloidal flux (and the associated current density) shown in Fig. 2. The peak of toroidal current density in the current layer is about  $500 \text{ kA/m}^2$  in the region of the high toroidal field side ( $B_\phi = 0.7 \text{ T}$ ) as shown in Fig. 2(b). In 3-D, non-axisymmetric magnetic fluctuations arise due to current-sheet instabilities localized near the edge region. Figure 3 shows the magnetic energy of different toroidal mode numbers during nonlinear evolution. As it is seen, magnetic fluctuations with low toroidal mode numbers  $n=1-6$  are linearly unstable and saturate, while fluctuations with higher toroidal modes numbers grow only nonlinearly and saturate at much lower amplitudes. The mode with the largest wavelength,  $n=1$ , grows with a growth rate of  $\gamma\tau_A = 0.086$  and also that with  $n=2-6$  grows fast. Here,  $\tau_A$  is the poloidal transit time based on the local reconnecting field  $B_z \approx 0.1 \text{ T}$ . The linear mode structure of the nonaxisymmetric mode,  $n=1$ , is shown in Fig. 3. This mode is localized around the edge current sheet (the edge region with the current density spike) and has a tearing parity (radial magnetic and velocity magnetic fluctuations are even and odd around the current layer, respectively).<sup>12</sup> The radial velocity changes its sign in the current layer, similar to peeling mode structures with tearing parity observed near the X point region reported in Ref. 22. As it is seen, this mode has a high poloidal mode number. Considering periodicity in the poloidal direction, this is expected in the edge region with a high winding number  $q = rB_\phi/RB_p = m/n$ . A similar current-driven  $n=1$  mode with a high poloidal mode number structure was also

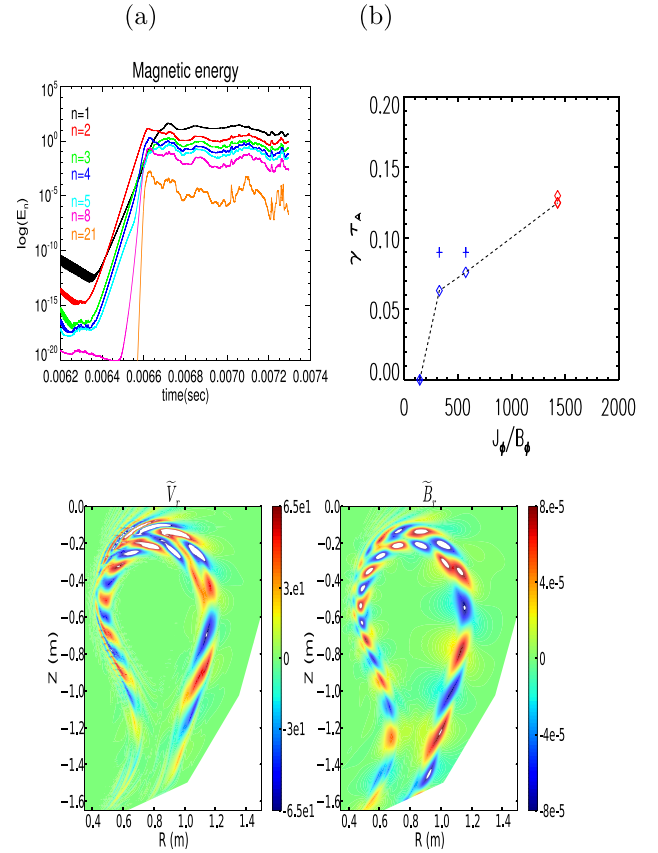


FIG. 3. Top left: Total magnetic energies of different toroidal mode numbers vs. time during nonlinear 3-D simulations ( $\eta = 5 \text{ m}^2/\text{s}$ ,  $B_\phi = 0.7 \text{ T}$ , peaked current density near the edge  $J_\phi = 500 \text{ kA/m}^2$ , and reconnecting field  $B_z = 0.1 \text{ T}$ ). Top right: Growth rates ( $\gamma\tau_A$ ) of  $n=1$  modes vs.  $J_\phi/B_\phi$  [ $\text{kA}/(\text{m}^2\text{T})$ ]. The three blue diamond (cross) points are  $n=1$  ( $n=2$ ) growth rates when the peak current density is fixed ( $J_\phi = 400 \text{ kA/m}^2$ ) and only the toroidal field is varied ( $B_\phi = 2.8, 1.23, \text{ and } 0.7 \text{ T}$ ) ( $S = 11\,000$ ). Red diamonds are  $n=1$  growth rates for  $J_\phi = 1 \text{ MA/m}^2$  and  $B_\phi = 0.7$  ( $\eta = 2.5, 8 \text{ m}^2/\text{s}$ ). Bottom: typical linear mode structures, radial velocity, and magnetic perturbations of the edge localized  $n=1$  mode.

triggered in simulations with different initial conditions for a specific case of CHI in NSTX.<sup>23</sup>

### III. GROWTH PHASE OF RECONNECTING EDGE LOCALIZED MODES

Next, to further investigate the nature of these edge localized modes, we perform several simulations by varying the toroidal field but with the same current density profile. We calculate the growth rates of these modes in the early linear phase of these nonlinear simulations. The first three points in Fig. 3(b) show the growth rates for simulations with three different toroidal fields. The peak toroidal current density (and its profile) in the edge current layer is kept the same ( $J_\phi = 400 \text{ kA/m}^2$ ). At a high toroidal guide field and low values of  $J_\phi/B_\phi$ , the edge localized current-driven  $n=1$  modes are stable. The instability grows fast at higher values of about  $J_\phi/B_\phi > 150 - 200$  as shown in Fig. 3(b). The scaling of the instability with  $J_\phi/B_\phi$  is consistent with the instability drive for the traditional ideal peeling modes,  $qRJ_\parallel/B$ .<sup>3</sup> However, here in the presence of resistivity which leads to a resolved physical current sheet, the criteria for the instability will be different from the ideal peeling mode stability

criteria. In the presence of resistivity, physical current layers developing near the plasma edge can be unstable to a 3-D current-sheet instability.<sup>12</sup> As the unstable mode here has reconnecting tearing parity, linear analysis for current-sheet instability such as oblique plasmoid instability<sup>24</sup> is therefore more relevant. Our limited scaling study for three  $S$  values in the range of  $(1 - 4 \times 10^5)$  shows a weak dependency on  $S$ . There is an opportunity for further linear theory development for the tokamak edge current sheet equilibrium profiles, for example incorporation of the edge current sheet width scaling with  $S$  into the tearing analysis for tokamak edge modes.

#### IV. FORMATION OF 3-D COHERENT STRUCTURES

Following the linear stage studied above, the modes saturate as shown in the magnetic energy evolution in Fig. 3(a). Fig. 4 shows the saturated nonlinear current density for the case above (with energy shown in Fig. 3) at  $t = 7$  ms. As seen, coherent non-axisymmetric  $n = 1$  structures have evolved during the nonlinear saturated state. These nonaxisymmetric structures break the initial axisymmetric current density (Fig. 2)(b). The edge localized modes with a low toroidal mode number saturate with magnetic perturbations with amplitudes of about a few percent of  $n = 0$  reconnecting the magnetic field (0.1 T). However, because of the very localized nature of the magnetic fluctuations, the amplitude of the associated perturbed toroidal current density can be as high as 50% of the  $n = 0$  component. For comparison, the nonlinear structure in simulations with only two toroidal Fourier modes and the linear structure are shown in Fig. 4

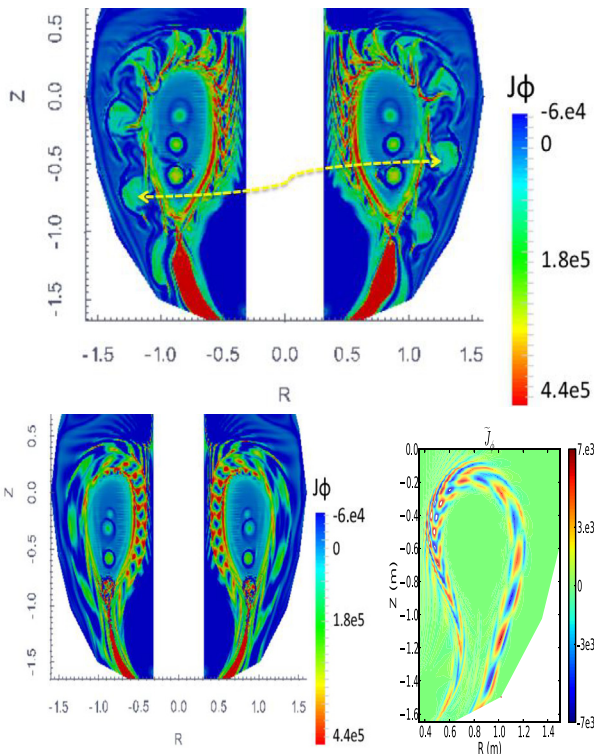


FIG. 4. Poloidal R-Z cuts of saturated nonlinear toroidal current density for the case shown in Fig. 3(a) at  $t = 7$  ms, top: with 22 toroidal Fourier modes and bottom left: with only 2 toroidal Fourier modes. Bottom right: linear toroidal current density mode structure in the growth phase of  $n = 1$ .

(lower panel). The radially propagating filament  $n = 1$  structures can only become coherent as the number of toroidal modes increased as seen in Fig. 4(a). The nonlinear filament structures are radially extended about 30–35 cm (Fig. 4(a)), while the linear mode structure has only a radial extension of about 10–15 cm (Fig. 4(c)).

As the poloidal flux is expanded into the whole volume, the injector voltage, the contributing source term of helicity injection, is turned off. This would induce an effective reconnection near the injection region, and a single X point configuration would eventually form as shown in Fig. 5. As seen from both the poloidal cut of toroidal current density and the puncture plot, an equilibrium state with closed flux surfaces is fully formed non-inductively while the injection source is absent ( $V_{inj} = 0$ ). The puncture plot obtained from the 3-D simulations shows the last closed flux surface (LCFS) extending radially from  $r = 0.52$  m–1.26 m (Fig. 5(b)). Figure 5(b) also shows a stochastic region outside of the separatrix. As observed from the current density plot in Fig. 5(a), the non-axisymmetric nonlinear mode structure radially extends from the closed flux region to the region of open field lines (outside of separatrix). The axisymmetric current density layer is strongly affected by the mode, is broken near the edge region of the closed flux surface, and is radially expanded in the form of coherent filaments.

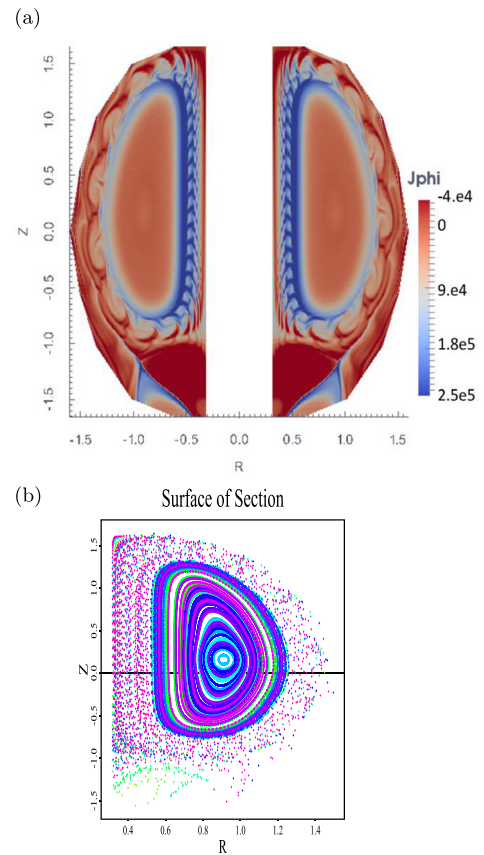


FIG. 5. (a) Poloidal R-Z cut of saturated nonlinear toroidal current density for the case shown in Fig. 3(a) at  $t = 8.56$  ms after the injection phase (injector voltage is not applied and is turned off at  $t = 8.1$  ms). At this time, an equilibrium state with closed flux surfaces is formed. (b) Poincare plots show the intersections of a field line with a poloidal plane, as the field line is followed around the torus at the same time in (a),  $t = 8.56$  ms, during the nonlinear 3-D simulation.

These localized coherent nonaxisymmetric structures are also nonlinearly formed due to the strong edge current layer in other simulations with different initial poloidal fluxes and higher peaked current density and S. Also, similar dynamics is found for the case at a higher density of  $10^{19} \text{m}^{-3}$  and with lower magnetic diffusivity (equivalent to higher temperature). The nonlinear dynamics of these structures for simulations at a higher toroidal field will be addressed below. All the cases exhibit some cycles. However, we present a case that has been run longer and exhibits more pronounced repetitive cycles.

## V. REPETITIVE CYCLES AND THE RELAXATION DYNAMICS

The observed edge localized coherent structures exhibit repetitive cycles during the nonlinear stage (top panel in Fig. 6). We now analyze the behavior of the nonlinear localized edge coherent structure during a cycle. The top panel of Fig. 6 shows the total energy vs. time during full nonlinear 3-D simulations with 43 toroidal modes and with a high toroidal field ( $B_\phi = 1.23 \text{T}$ ). We study the nonlinear dynamics during the flat top part of the total current (320 kA). Axisymmetric edge toroidal current layers are formed poloidally (on both the low field and high field sides). However, due to the high toroidal field, only the outer edge (on the low field side) remains strongly perturbed (as shown in Fig. 6). The lower panel of Fig. 6 shows the poloidal cross-sections of nonlinear total toroidal current densities at two conditions, at maximum ( $t = 8.8 \text{ms}$ ) and minimum ( $t = 8.7 \text{ms}$ ) fluctuations, during a cycle. At

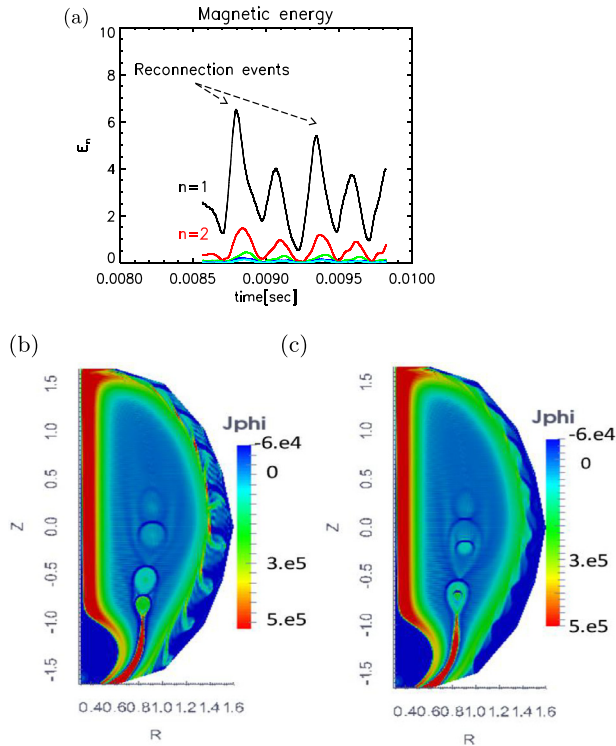


FIG. 6. Top: Cyclic oscillations of total magnetic energies of edge localized modes during nonlinear 3-D simulations in NSTX-U geometry with  $B_\phi = 1.23 \text{T}$ . Poloidal R-Z cuts of saturated nonlinear toroidal current density at  $t = 8.8 \text{ms}$  (bottom left) and  $t = 8.7 \text{ms}$  (bottom right).

the condition with a maximum fluctuation level, edge localized modes evolve to form coherent nonlinear filament structures at the low field side (lower panel Fig. 6). These localized current carrying structures with poloidally (twisting vertically) and toroidally ( $n = 1$  wrapping around the torus) localization are also extended radially. The structures do relax back radially to merge back into an axisymmetric toroidal current density as seen in Fig. 6 (lower right panel) near the edge region of the low field side. Note that the axisymmetric plasmoids generated during helicity injection as seen in Fig. 6 have been studied elsewhere.<sup>12</sup> Here, the focus is the coherent *edge* localized structures.

We examine these relaxation events by analyzing the fluctuation induced emf term (the correlated flow and magnetic field fluctuations  $\tilde{\mathbf{V}} \times \tilde{\mathbf{B}}$ ) from the edge localized modes themselves. The fluctuations can affect the total current in two ways: by reaching a finite amplitude and by modifying the average current density through the mean emf dynamo term. We separate the fields into mean and fluctuating components ( $\mathbf{J} = \langle \mathbf{J} \rangle_{n=0} + \tilde{\mathbf{J}}_{n \neq 0}$ ), where mean  $\langle \rangle$  is the vertically and toroidally ( $Z, \phi$ ) averaged axisymmetric field. The coherent nonaxisymmetric structures with high poloidal mode numbers (as the edge localized modes themselves) create current holes in the current layer as seen in the low field side (Fig. 6(b)) and relax back (Fig. 6(c)). The modification of the edge current density and the formation of current holes can be explained through the mean fluctuation induced emf.

Figure 7 shows the toroidal current density averaged vertically (averaged around midplane  $-0.5 \text{m} < Z < +0.5 \text{m}$ ) at two conditions. During the low fluctuation part of the cycle ( $t = 8.7 \text{ms}$ ), the current density remains mostly axisymmetric, with the positive spike of the current (radially symmetric at around  $R = 1.35 \text{m}$ ), as shown in Fig. 7(a). However, the vertically averaged current density is drastically different because of the nonaxisymmetric fluctuations at  $t = 8.8 \text{ms}$ , and a current hole region at around  $R = 1.38 - 1.45 \text{m}$  is created (red curve in Fig. 7(a)). The calculated toroidal fluctuation induced emf,  $\langle \tilde{\mathbf{V}} \times \tilde{\mathbf{B}} \rangle_\phi = 1/2 R e [\tilde{V}_r \tilde{B}_z^* - \tilde{V}_z \tilde{B}_r^*]$ , at these two conditions is also shown in Fig. 7(b). As seen, a nonzero fluctuation induced nonlinear dynamo term is bipolar and has a sufficiently large amplitude to contribute to the current density modification. The localized dynamo term changes its sign around the same radius where the flattening and annihilation of current density occur. It is therefore shown that the emf does contribute to the formation of current holes and the

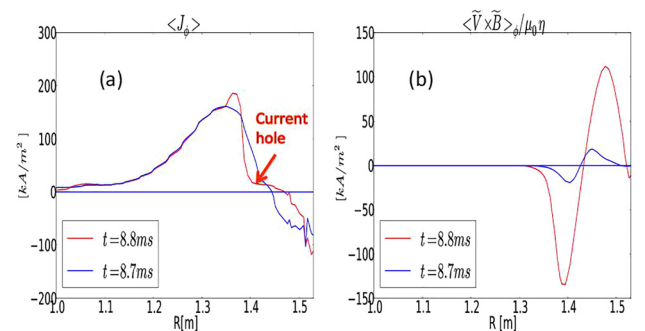


FIG. 7. Profiles of (a)  $\langle J_\phi \rangle$  averaged vertically and (b) normalized ( $R, \phi$ )-averaged toroidal emf term  $\langle \tilde{\mathbf{V}} \times \tilde{\mathbf{B}} \rangle_\phi$ , at two times during a cycle.

radially outward expulsion of the current density. It should be noted that the relaxation in a short time period of 0.1 ms, shown in Figs. 6 and 7, is consistent with the experimentally observed time scales.

## VI. SUMMARY AND DISCUSSION

In conclusion, nonlinear coherent filament edge localized structures have been formed during the full nonlinear 3-D resistive MHD simulations in a tokamak configuration. The structures are nonaxisymmetric, poloidally localized, wrapped around the torus, and radially extended. The mode structure in the closed flux region extends to the open field region during the nonlinear evolution. For the first time, it has been shown that the edge localized structures in tokamaks (1) have reconnecting nature, (2) grow much faster (close to poloidal Alfvén transit times) than the global tearing modes,<sup>25</sup> and (3) have a finite localized fluctuation-induced bi-directional emf dynamo term ( $\langle \tilde{\mathbf{V}} \times \tilde{\mathbf{B}} \rangle$ ), which could cause the local annihilation of axisymmetric current (current holes) near the edge region in the nonlinear stage. The coherent filament structures found here are very similar to the camera images of peeling modes from the Pegasus spherical tokamak (see Fig. 1 in Ref. 8).

Our simulations also show the existence of non-axisymmetric total toroidal current density in the edge region (both around the separatrix and the open field line regions). We have shown that the peak current density relaxation near the edge can play a contributing role in the cyclic oscillations of low- $n$  peeling-type ELMs. Recent measurements show that high frequency magnetic fluctuations are correlated with the inter-ELMs in ASDEX Upgrade. The associated current fluctuations are measured on both the low and high field sides, indicating a strong peeling/current-driven part.<sup>26</sup> It is also shown that inter-ELM modes with toroidal structures in the range of  $n = 1 - 10$  cause transport across the pedestal.<sup>27</sup> Our simulations here highlight the role of edge current relaxation and could shed light on the dynamics of MHD mode activity during ELM cycles. We should further stress that the creation of non-axisymmetric edge current density in our simulations occurs both (1) while the magnetic flux bubble is expanding in the volume, i.e., the plasma being vertically displaced upward, and (2) in the flat top phase of current while a quasi-steady equilibrium state is formed. In both the phases, 3-D fluctuations form non-axisymmetric current-density coherent ELM filaments. The former however is also relevant to edge/wall currents induced due to vertical displacement events (VDEs) during disruption.<sup>28</sup> We propose a scenario such that as the plasma is vertically displaced, edge induced plasma current becomes MHD peeling-tearing unstable and forms non-axisymmetric coherent edge current structures, which would eventually bleed into the walls.

It should also be stressed that to shed light onto the role of reconnection in ELM nonlinear filament dynamics, we have isolated the effect of edge current density gradients by not evolving the pressure. In our model, by suppressing the instabilities arising from the pressure gradient, we have been able to capture the essential reconnection physics in the edge region of tokamaks. In addition, our model has shown itself

to be able to reproduce low- $n$  ELM peeling-driven filament structures, which have also been experimentally observed.<sup>8</sup> In conventional tokamaks, ELMs are mostly known to be triggered as the critical pressure gradient is exceeded. Most of the theoretical studies have so far been linear or nonlinear reduced MHD<sup>29</sup> and have been based on the ideal high- $n$  ELMs with interchange/ballooning characteristics. Nonlinear reduced MHD simulations have also been used to simulate  $n = 1$  peeling-tearing modes.<sup>30</sup>

Full nonlinear MHD studies with a high toroidal mode number resolution such as this study are required to recognize the role of reconnection in the low- $n$  as well as high- $n$  ELM simulations. The current spikes near the edge can trigger 3-D current-sheet instabilities, which have growth rates faster than the global tearing modes. But unlike the ideal modes, these modes have tearing characteristics, which means that they allow reconnection on short time scales. This is analogue to plasmoid tearing instability, which grows on Alfvénic time scales, but does have reconnecting nature.<sup>31,32</sup> We therefore here by having only current-gradient component, i.e., peeling-tearing instabilities alone were able to track the reconnection process and relaxation due to the current-sheet instabilities. Also, our preliminary simulation where we have included pressure evolution shows that the dynamics are more complicated, but reconnection does still play an important role in the nonlinear dynamics.

In summary, edge current-sheets/spikes can develop in the edge region under different circumstances such as (1) during flux expansion during helicity injection (CHI), (2) as a peeling component of ELMs—bootstrap currents, (3) due to the strong current ramp up as in the case of peeling modes from the Pegasus spherical tokamak,<sup>8</sup> and (4) during vertical displacement events—the scrape-off layer currents (halo currents). In all these cases, edge current-sheets can become unstable to nonaxisymmetric 3-D current-sheet instabilities and nonlinearly form edge coherent current-carrying filaments (also referred to as 3-D plasmoids or current-carrying blobs in the scrape-off layer) as shown in our simulations. In this study, by utilizing the helicity injection technique to form a large finite edge current density, we have focused on the governing dynamics of low- $n$  current-driven peeling ELMs. To study these nonlinear filaments, we have indeed pushed the parameters (to the so-called strongly driven CHI regime) to trigger the low- $n$  ELMs to saturate at large amplitudes. The direct application of these results for the specific optimization of transient CHI for startup with the relevant parameter regime will be presented in a separate paper. There, using the narrow flux footprint and the parameter range of NSTX-U (at a higher toroidal field), it will be reported that even in the presence of nonaxisymmetric edge magnetic fluctuations, large-volume flux closure is formed in transient CHI. The results of our previous axisymmetric study<sup>11</sup> for maximum flux closure and CHI generated closed-flux will be extended to include 3-D fluctuations.

Finally, as solar eruptions are accompanied by the ejection of field-aligned filamentary structures into the surrounding space, the MHD study of nonlinear filaments here could also improve our understanding of these eruptive events on the sun. The 3-D current-carrying filament structures and

their nonlinear dynamics due to the dynamo effect are relevant to flares, which also exhibit complicated magnetic flux tube dynamics.

## ACKNOWLEDGMENTS

We acknowledge S. Prager and R. Raman for valuable comments on this Manuscript, and L. Comisso for useful discussions. Computations were performed at NERSC. This work was supported by DOE Grant Nos. DE-SC0010565, DE-AC02-09-CH11466, and DE-SC0012467.

- <sup>1</sup>M. Shimada, D. J. Campbell, V. Mukhovatov, M. Fujiwara, N. Kirneva, K. Lackner, M. Nagami, V. D. Pustovitov, N. Uckan, J. Wesley *et al.*, *Nucl. Fusion* **47**, S1 (2007).
- <sup>2</sup>F. Wagner, G. Becker, K. Behringer, D. Campbell, A. Eberhagen, W. Engelhardt, G. Fussmann, O. Gehre, J. Gernhardt, G. V. Gierke *et al.*, *Phys. Rev. Lett.* **49**, 1408 (1982).
- <sup>3</sup>J. W. Connor, *Plasma Phys. Controlled Fusion* **40**, 531 (1998).
- <sup>4</sup>P. B. Snyder, H. R. Wilson, J. R. Ferron, L. L. Lao, A. W. Leonard, T. H. Osborne, A. D. Turnbull, D. Mossessian, M. Murakami, and X. Q. Xu, *Phys. Plasmas* **9**, 2037 (2002).
- <sup>5</sup>H. R. Wilson, P. B. Snyder, G. T. A. Huysmans, and R. L. Miller, *Phys. Plasmas* **9**, 1277 (2002).
- <sup>6</sup>N. M. Ferraro, S. C. Jardin, and P. B. Snyder, *Phys. Plasmas* **17**, 102508 (2010).
- <sup>7</sup>B. J. Burke, S. E. Kruger, C. C. Hegna, P. Zhu, P. B. Snyder, C. R. Sovinec, and E. C. Howell, *Phys. Plasmas* **17**, 032103 (2010).
- <sup>8</sup>M. W. Bongard, R. J. Fonck, C. C. Hegna, A. J. Redd, and D. J. Schlossberg, *Phys. Rev. Lett.* **107**, 035003 (2011).
- <sup>9</sup>A. Kirk, B. Koch, R. Scannell, H. R. Wilson, G. Counsell, J. Dowling, A. Herrmann, R. Martin, and M. Walsh, *Phys. Rev. Lett.* **96**, 185001 (2006).
- <sup>10</sup>R. Maingi, M. G. Bell, E. D. Fredrickson, K. C. Lee, R. J. Maqueda, P. Snyder, K. Tritz, S. J. Zweben, R. E. Bell, T. M. Biewer *et al.*, *Phys. Plasmas* **13**, 092510 (2006).
- <sup>11</sup>F. Ebrahimi and R. Raman, *Nucl. Fusion* **56**, 044002 (2016).
- <sup>12</sup>F. Ebrahimi, *Phys. Plasmas* **23**, 120705 (2016).
- <sup>13</sup>K. Kusano, T. Maeshiro, T. Yokoyama, and T. Sakurai, *Astrophys. J.* **610**, 537 (2004).
- <sup>14</sup>K. Kusano, T. Maeshiro, T. Yokoyama, and T. Sakurai, *Astrophys. J.* **577**, 501 (2002).
- <sup>15</sup>J. Warnecke and A. Brandenburg, *Astron. Astrophys.* **523**, A19 (2010).
- <sup>16</sup>T. Török, B. Kliem, and V. S. Titov, *Astron. Astrophys.* **413**, L27 (2004). astro-ph/0311198.
- <sup>17</sup>W. J. Hughes and D. G. Sibeck, *Geophys. Res. Lett.* **14**, 636, doi:10.1029/GL014i006p00636 (1987).
- <sup>18</sup>F. Ebrahimi and R. Raman, *Phys. Rev. Lett.* **114**, 205003 (2015).
- <sup>19</sup>C. R. Sovinec, A. H. Glasser, T. A. Gianakon, D. C. Barnes, R. A. Nebel, S. E. Kruger, D. D. Schnack, S. J. Plimpton, A. Tarditi, M. Chu *et al.*, *J. Comput. Phys.* **195**, 355 (2004).
- <sup>20</sup>F. Ebrahimi, E. B. Hooper, C. R. Sovinec, and R. Raman, *Phys. Plasmas* **20**, 090702 (2013).
- <sup>21</sup>E. B. Hooper, C. R. Sovinec, R. Raman, F. Ebrahimi, and J. E. Menard, *Phys. Plasmas* **20**, 092510 (2013).
- <sup>22</sup>G. T. A. Huysmans, *Plasma Phys. Controlled Fusion* **47**, 2107 (2005).
- <sup>23</sup>E. Hooper and C. Sovinec, *Phys. Plasmas* **23**, 102502 (2016).
- <sup>24</sup>S. D. Baalrud, A. Bhattacharjee, and Y.-M. Huang, *Phys. Plasmas* **19**, 022101 (2012).
- <sup>25</sup>H. P. Furth, J. Killeen, and M. N. Rosenbluth, *Phys. Fluids* **6**, 459 (1963).
- <sup>26</sup>F. M. Laggner, E. Wolfrum, M. Cavedon, F. Mink, E. Viezzer, M. G. Dunne, P. Manz, H. Doerk, G. Birkenmeier, R. Fischer *et al.*, *Plasma Phys. Controlled Fusion* **58**, 065005 (2016).
- <sup>27</sup>F. Mink, E. Wolfrum, M. Maraschek, H. Zohm, L. Horváth, F. M. Laggner, P. Manz, E. Viezzer, U. Stroth, and the ASDEX Upgrade Team, *Plasma Phys. Controlled Fusion* **58**, 125013 (2016).
- <sup>28</sup>S. P. Gerhardt, J. Menard, S. Sabbagh, and F. Scotti, *Nucl. Fusion* **52**, 063005 (2012).
- <sup>29</sup>F. Orain, M. Bécoulet, G. T. A. Huysmans, G. Dif-Pradalier, M. Hoelzl, J. Morales, X. Garbet, E. Nardon, S. Pamela, C. Passeron *et al.*, *Phys. Rev. Lett.* **114**, 035001 (2015).
- <sup>30</sup>G. T. A. Huysmans and O. Czarny, *Nucl. Fusion* **47**, 659 (2007).
- <sup>31</sup>F. Pucci and M. Velli, *Astrophys. J. Lett.* **780**, L19 (2014).
- <sup>32</sup>L. Comisso, M. Lingam, Y.-M. Huang, and A. Bhattacharjee, *Phys. Plasmas* **23**, 100702 (2016).